Biochemistry

pubs.acs.org/biochemistry Article

IpdE1-IpdE2 Is a Heterotetrameric Acyl Coenzyme A Dehydrogenase That Is Widely Distributed in Steroid-Degrading Bacteria

John E. Gadbery, James W. Round, Tianao Yuan, Matthew F. Wipperman, Keith T. Story, Adam M. Crowe, Israel Casabon, Jie Liu, Xinxin Yang, Lindsay D. Eltis,* and Nicole S. Sampson*

Cite This: *Biochemistry* 2020, 59, 1113−1123 Read Online

ACCESS | Metrics & More | Article Recommendations | Supporting Information

ABSTRACT: Steroid-degrading bacteria, including *Mycobacterium tuberculosis* (*Mtb*), utilize an architecturally distinct subfamily of acyl coenzyme A dehydrogenases (ACADs) for steroid catabolism. These ACADs are $\alpha_2\beta_2$ heterotetramers that are usually encoded by adjacent *fadE*-like genes. In mycobacteria, *ipdE1* and *ipdE2* (formerly *fadE30* and *fadE33*) occur in divergently transcribed operons associated with the catabolism of 3a*α*-*H*-4*α*(3′-propanoate)-7a*β*-methylhexahydro-1,5-indanedione (HIP), a steroid metabolite. In *Mycobacterium smegmatis*, Δ*ipdE1* and Δ*ipdE2* mutants had similar phenotypes, showing impaired growth on cholesterol and accumulating 5-OH HIP in the culture supernatant. Bioinformatic analyses revealed that IpdE1 and IpdE2 share many of the features of the *α*- and *β*-subunits, respectively, of heterotetrameric ACADs that are encoded by adjacent genes in many steroid-degrading proteobacteria. When coproduced in a rhodococcal strain, IpdE1 and IpdE2 of *Mtb* formed a complex that catalyzed the dehydrogenation of 5OH-HIP coenzyme A (5OH-HIP-CoA) to 5OH-3a*α*-*H*-4*α*(3′-prop-1-enoate)-7a*β*-methylhexahydro-1,5-indanedione coenzyme A ((*E*)-5OH-HIPE-CoA). This corresponds to the initial step in the pathway that leads to degradation of steroid C and D rings via *β*-oxidation. Small-angle X-ray scattering revealed that the IpdE1-IpdE2 complex was an $\alpha_2\beta_2$ heterotetramer typical of other ACADs involved in steroid catabolism. These results provide insight into an important class of steroid catabolic enzymes and a potential virulence determinant in *Mtb*.

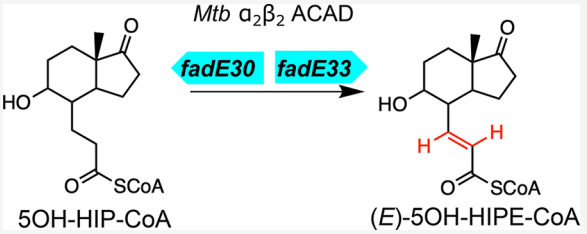

Bacteria are the only organisms known to utilize steroids as growth substrates.[1] This catabolism has been studied for many decades, due in part to its potential to transform low-value steroids into high-value pharmaceutical reagents.[2] However, steroid catabolism is also an important process for biomass decomposition, and a recent metagenomic study identified a number of actinobacterial and proteobacterial lineages of steroid degraders.[1] In addition, the cholesterol catabolic pathway of *Mycobacterium tuberculosis* (*Mtb*), the infectious agent responsible for tuberculosis (TB), has been studied due to its role in virulence.[3,4] *Mtb* infects one-third of the world's population and results in 1.6 million deaths worldwide per year.[5] Cholesterol catabolism is required for the survival of *Mtb* in macrophages and is a potential target for novel therapeutics that are urgently needed to treat TB.[6,7] Despite the intensified research, many aspects of steroid catabolism remain unclear.

Studies of steroid catabolism in *Rhodococcus jostii* RHA1 (*R. jostii* RHA1), *Mtb*, and *Comamonas testosteroni* TA441 indicate that this catabolism largely follows the structural elements of the steroid molecule: first, the alkyl side chain when present, then Rings A/B followed by Rings C/D, respectively (Figure 1).[8−11] Side-chain degradation resembles the *β*-oxidation of fatty acids.[12] A cytochrome P450 (Cyp125[13] or Cyp142[14]) catalyzes oxidation of a terminal methyl to a carboxylic acid, and after conversion to a CoA thioester, *β*-oxidation of the side chain generates propionyl- and acetyl-CoA.[15,16] Rings A/B-degradation includes oxygenases that catalyze the 9,10-cleavage of the steroid nucleus and the 4,5-extradiol cleavage of ring A, respectively.[17−19] In *Mtb* and other Actinobacteria, genes encoding cholesterol uptake, side-chain and rings A/B degradations are transcriptionally regulated by KstR, a TetR-family repressor,[20] and side-chain and rings A/B degradations occur concurrently to at least some extent.[21] In all aerobic steroid-degrading bacteria characterized to date, catabolism yields 3a*α*-*H*-4*α*(3′-propanoate)-7a*β*-methylhexahydro-1,5-indanedione (HIP),[22,23] a 13-carbon catabolite containing intact rings C/D, or a derivative thereof (Figure 1). HIP is catabolized to central metabolites by a conserved *β*-oxidation pathway encoded by 13 genes.[10] In *Mtb* and other Actinobacteria, these genes are regulated by KstR2.[24]

Acyl coenzyme A (acyl-CoA) dehydrogenases (ACADs) are a class of flavoenzymes that play an important role in *β*-oxidation, catalyzing the initial transformation of the acyl-CoA

Received: January 2, 2020
Revised: February 20, 2020
Published: February 26, 2020

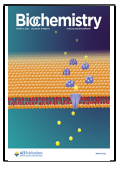

https://dx.doi.org/10.1021/acs.biochem.0c00005
Biochemistry 2020, 59, 1113−1123

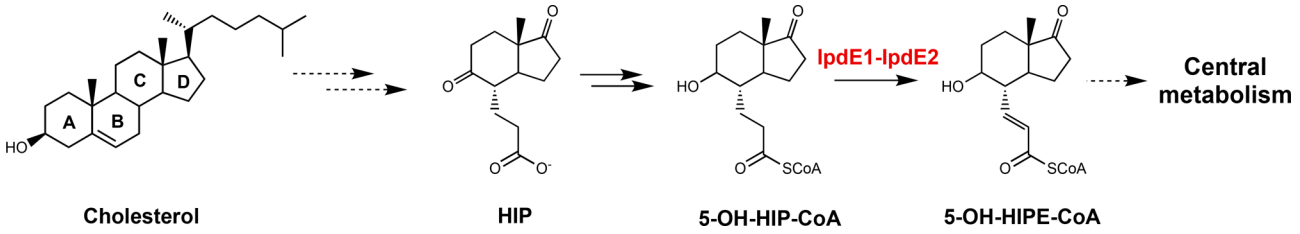

Figure 1. Role of IpdE1-IpdE21 (FadE30-FadE33) in the cholesterol catabolic pathway. Cholesterol is catabolized to HIP via degradation of the steroid side chain and rings A and B. HIP is transformed to 5-OH-HIP by the successive actions of FadD3 and IpdF. IpdE1-IpdE2 (FadE30-FadE33) is proposed to catalyze the oxidation of 5-OH-HIP-CoA to 5OH-HIPE-CoA, which undergoes further β-oxidative degradation to central metabolites.

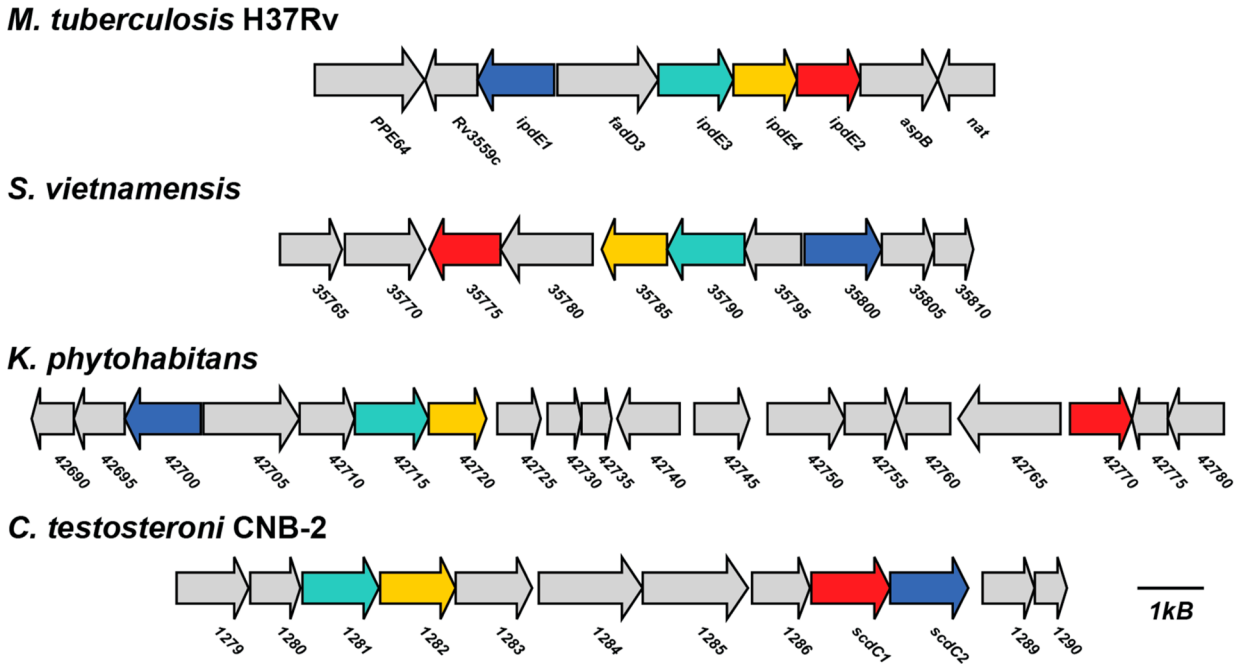

Figure 2. Synteny of *ipdE* genes in diverse bacteria. The occurrence of orthologs of the Mtb *ipdE* genes (colored as indicated in the top row) in three representative actinobacteria and a β-proteobacterium, *Comamonas testosteroni* CNB-2. ORFs in *Streptomyces vietnamensis*, *Kibdelosporangium phytohabitans*, and *C. testosteroni* CNB-2 have the prefixes SVTN_, AOZ06_, and CtCNB1_, respectively.

to an enoyl-CoA in each cycle of this process.[25] They possess the same structural fold, suggesting a shared evolutionary origin. These enzymes are typically homotetramers with four flavin adenine dinucleotide (FAD) cofactors and four active sites. An architecturally distinct class of $\alpha_2\beta_2$ ACADs was recently identified in the cholesterol catabolic pathway of *Mtb*.[26,27] The α- and β-subunits of these heterotetrameric enzymes are homologous and are encoded by tandem *fadE* genes that occur in an operon (Figure 2).[26,28] The best characterized $\alpha_2\beta_2$ ACADs are ChsE1-ChsE2 (FadE28-FadE29 in *R. jostii* RHA1) and ChsE4-ChsE5 (FadE26-FadE27 in *R. jostii* RHA1) that catalyze the dehydrogenation of 3-oxo-4-pregnene-20-carboxyl-CoA and 3-oxo-cholest-4-en-26-oyl CoA, respectively, in cholesterol side-chain degradation.[26,28] ChsE1-ChsE2 and ChsE4-ChsE5 are $\alpha_2\beta_2$ heterotetramers based on molecular weight and oligomeric stoichiometry, and the X-ray crystallographic structure of ChsE4-ChsE5 has been determined.[28] Although the α- and β-subunits are homologous, each $\alpha\beta$ protomer contains a single FAD and therefore has a single active site.[27,28]

The actinobacterial KstR2 regulon harbors four *fadE* genes: *fadE30*, *fadE31*, *fadE32*, and *fadE33* that are homologues of known $\alpha_2\beta_2$ ACADs. Due to their involvement in the catabolism of HIP,[10] we henceforth rename these genes *ipdE1*, *ipdE3*, *ipdE4*, and *ipdE2*, respectively, for consistency with the nomenclature of other HIP (methylhexahydroindanone propionate)-degrading genes.[29] In mycobacteria, *ipdE3* (*fadE31*), *ipdE4* (*fadE32*), and *ipdE2* (*fadE33*) occur in one operon while *ipdE1* (*fadE30*) occurs in an adjacent, divergently transcribed operon.[10] Transposon mutagenesis studies have suggested that *ipdE1* and *ipdE4* are essential for virulence of *Mtb* in macrophages and for chronic *Mtb* infection in mice.[30,31] IpdE3-IpdE4 forms a complex and has been proposed to catalyze the dehydrogenation of a CoA thioester of 4-methyl-5-oxo-octanedioate, a late intermediate of 5OH-HIP-CoA degradation.[10,27] In some Proteobacteria including *Comamonas testosteroni*, *ipdE1* and *ipdE2* occur in the same operon.[10] Based on gene deletion studies and bioinformatic analyses, homologues of IpdE1 and IpdE2 in *C. testosteroni* TA441 were predicted to form an ACAD involved in dehydrogenating 5OH-HIP-CoA to 5OH-HIPE-CoA.[32] In *Rhodococcus equi*, *ipdE1* is required for growth on 5OH-HIP, and a Δ*ipdE1* strain of *R. equi* accumulated large amounts of 5OH-HIP-CoA when grown on 4-androstene-3,17-dione.[29] Based on these data and the known heterotetrameric structures of other Actinobacterial ACADs,[27] we hypothesize that *ipdE1*

https://dx.doi.org/10.1021/acs.biochem.0c00005
Biochemistry 2020, 59, 1113−1123

and *ipdE2* encode an $\alpha_2\beta_2$ ACAD that catalyzes the dehydrogenation of 5OH-HIP-CoA to 5OH-HIPE-CoA.

Herein, we used molecular genetics to evaluate the roles of *ipdE1* and *ipdE2* in *M. smegmatis* and *Mtb*. We performed phylogenetic analyses to determine the relationship of IpdE1 to other bacterial FadEs. We then used *R. jostii* RHA1 as a host to heterologously produce IpdE1-IpdE2 of *Mtb*. We characterized the resulting enzyme biochemically and, using small-angle X-ray scattering (SAXS) analysis, structurally. The results are discussed in terms of steroid catabolism and other ACADs.

MATERIALS AND METHODS

Reagents. Enzymes for cloning were purchased from New England. Primers were ordered from Integrated DNA Technologies. Chemicals were of at least reagent grade unless otherwise noted. Buffers were prepared using water purified on a Barnstead GenPure Pro System (Thermo Scientific) to a resistivity of greater than 18 MΩcm. 5OH-HIP-CoA,[23] octanoyl-CoA,[26] dihydroferuloyl-CoA,[33] and 3-oxo-4-pregnene-20-carboxyl-CoA[11] were prepared as previously described.

Strains and Culture Conditions. *Escherichia coli* strains DH5α and BL21 were used to propagate DNA and produce protein, respectively. *E. coli* strains were routinely grown in LB broth at 37 °C, 200 rpm. *R. jostii* RHA1 was routinely grown in LB at 30 °C while shaking at 200 rpm. For protein production, *E. coli* BL21 and *R. jostii* RHA1 cells were grown in 2xYT medium supplemented with 0.02% (v/v) corn steep liquor. *Mycobacterium smegmatis* was grown in 7H9 medium containing 0.5% tyloxapol, supplemented with 0.1% glycerol or 1 mM cholesterol, at 37 °C and shaking at 200 rpm. *Mtb* CDC1551 *ipdE2*::Tn from BEI Resources was grown in 7H9 medium containing 0.5% tyloxapol, supplemented with 0.01% (w/v) cholesterol, at 37 °C in roller bottles. For solid medium, liquid broths were supplemented with Bacto agar (1.5% [w/v]; Difco). Media were further supplemented with antibiotics as follows: 100 μg/mL ampicillin for *E. coli* carrying pTip-derived plasmids; 34 μg/mL chloramphenicol, *R. jostii* RHA1 carrying pTip-derived plasmids; 150 μg/mL hygromycin, *E. coli* carrying pYUB854-derived plasmids; 50 μg/mL hygromycin, *M. smegmatis* deletion mutants; and 20 μg/mL kanamycin, *M. smegmatis* carrying pJV53.

DNA Manipulation. Oligonucleotides and plasmids used in this study are listed in Table S1 and S2, respectively. DNA was isolated, manipulated, and analyzed using standard protocols.[34] *E. coli*, *R. jostii* RHA1, and *M. smegmatis* cells were transformed using electroporation. The nucleotide sequence of constructs was verified.

Construction of *R. jostii* RHA1 Expression Vectors. To create expression vectors, *ipdE1* (*fadE30*, *Rv3560C*) and *ipdE2* (*fadE33*, *Rv3564*) were amplified from *Mtb* H37Rv genomic DNA, using primer pairs listed in Table S1, digested with *Nde*I/*Hind*III, and ligated into *Nde*I/*Hind*III-linearized pTipQC2[35] to yield pTip-*ipdE1*, pTip-His$_6$-*ipdE1* and pTip-His$_6$-*ipdE2*, respectively. To construct a coexpression vector for *ipdE1* and *His$_6$-ipdE2*, the *His$_6$-ipdE2* expression cassette, including the promoter, RBS, His$_6$-*ipdE2*, and terminator, was amplified from pTip-His$_6$-*ipdE2* using the co-pTip primer pair, and inserted into *Kpn*I-linearized pTip-*ipdE1* using Gibson Assembly to yield pTip-*ipdE1*/*His$_6$-ipdE2*. All constructs were sequence confirmed.

Gene Deletion. Genes were deleted in *M. smegmatis* using recombineering to replace target genes with *hyg^R* cassettes.[36] Briefly, regions flanking *msmeg_6012* and *msmeg_6016* (*ipdE1* and *ipdE2*, respectively) were amplified from *M. smegmatis* genomic DNA using the oligonucleotides listed in Table S1. Amplicons were cloned on either side of the *hyg^R* cassette in pYUB854 using the *Afl*II/*Xba*I and *Nhe*I/*Bgl*II restriction site pairs. The linearized allelic exchange substrates were electroporated into *M. smegmatis* containing pJV53. Homologous recombination events resulting in the deletion of each gene were confirmed using PCR.

Transformation of Cholesterol. Cultures of Δ*ipdE1*, Δ*ipdE2*, and Δ*ipdE4 M. smegmatis* were grown to mid log phase (OD_{600} = 0.6) in 7H9 media supplemented with 0.1% glycerol and harvested by centrifugation (4000*g*, 20 min at 16 °C). Cells were washed using M9 salts, then suspended in 50 mL M9 salts, 2 mM $MgSO_4$, 0.1 mM $CaCl_2$ and 0.5 mM cholesterol, and incubated at 37 °C for 24 h. Cells were harvested by centrifugation and discarded. The supernatant was acidified and extracted with an equal volume of ethyl acetate. Extracts were dried under nitrogen, suspended in pyridine, and derivatized with bis(trimethylsilyl)-trifluoroacetamide/trimethyl-chlorosilane.

Gas Chromatography−Coupled Mass Spectrometry (GC−MS). Derivatized extracts were analyzed using an Agilent 6890 series gas chromatograph equipped with a 30 m HP-5 ms column (Agilent) and an HP 5973 mass-selective detector. The GC injector was set at 280 °C and the transfer line at 290 °C, and the helium flow rate was 1 mL/min. The oven was held at 104 °C for 2 min, then increased to 290 °C at a rate of 15 °C/min, and held at 290 °C for 15 min.

Bioinformatic Analyses. For synteny analyses, multigene BLAST was performed in architecture search mode with default parameters against the GenBank BCT (bacterial sequence) database using the sequences of *Mtb* IpdE1 (Rv3560c, I6Y3 V5), IpdE3 (Rv3562, I6YGH7), IpdE4 (Rv3563, P96845), and IpdE2 (Rv3564, I6YCF5). Non-redundant model organisms from the top 1000 hits were chosen, and their operon structures were examined using the ggenes package of R.[37] Representative architectures were visualized with Gene Graphics.[38] Phylogenetic analyses of the ACADs was performed using the NGPhylogeny.fr workflow.[39] Briefly, amino acid sequences (Table S3) were aligned using MUSCLE,[40] curated with trimAl,[41] and a phylogenetic tree was generated with PhyML 3.0 using the LG substitution model and aLRT (SH-like) statistics.[42]

Expression and Purification of IpdE1-IpdE2. *R. jostii* RHA1 transformed with pTip-*ipdE1*/*His$_6$-ipdE2* was inoculated into 2xYT medium supplemented with 0.02% (v/v) corn steep liquor. Cultures were incubated at 30 °C with shaking at 250 rpm, induced with 20 μg/mL thiostrepton when the OD_{600} reached 0.3−0.6, and allowed to grow for an additional 24 h. The cells were pelleted by centrifugation at 4500*g* for 20 min and suspended in eight volumes of 20 mM MOPS, 200 mM NaCl, 1 mM EDTA acid, 1 mM DTT, 10% glycerol, pH 7.5, supplemented with completeMini protease inhibitor (Millipore-Sigma). The cells were lysed by passing them four times at 27,000 psi through a Constant Systems E1061 cell disruptor (Daventry). Cell debris was removed by centrifugation at 50,000*g* for 60 min. Clarified lysate was loaded onto a 5 mL Ni-NTA resin pre-equilibrated with 10 mM imidazole, 20 mM $NaHPO_4$, 500 mM NaCl, pH 7.4, washed with 10 column volumes (CV) of this same buffer and 10 CV of 30 mM imidazole, 20 mM $NaHPO_4$, 500 mM NaCl, pH 7.4. Bound protein was eluted with 5 CV of 200 mM imidazole, 20 mM

https://dx.doi.org/10.1021/acs.biochem.0c00005
Biochemistry 2020, 59, 1113−1123

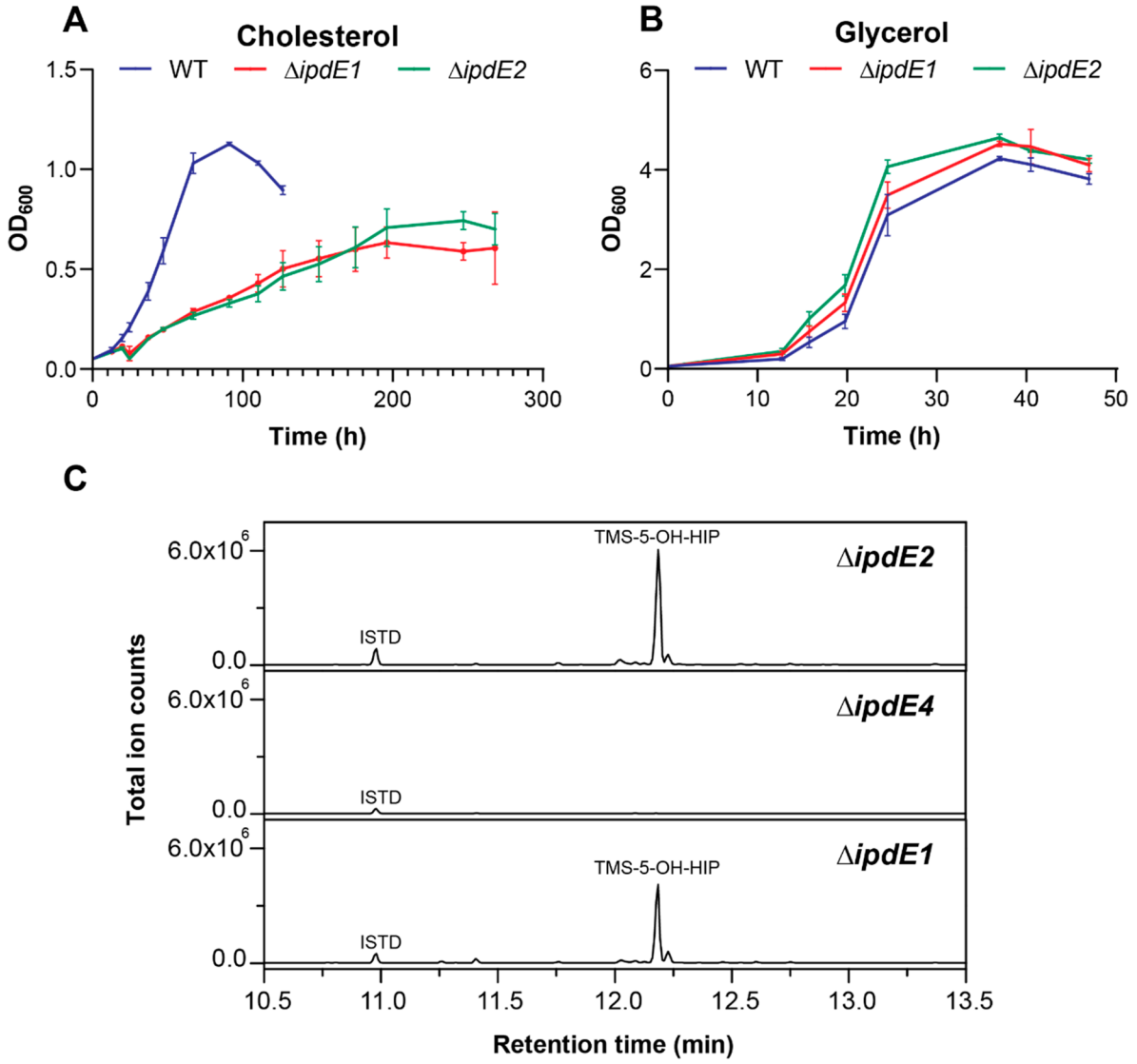

Figure 3. Phenotype of the *ipdE* mutants. Growth of *M. smegmatis* strains on 7H9 medium with 0.5% tyloxapol supplemented with either (A) 1 mM cholesterol or (B) 0.1% glycerol. Growth curves represent the mean of biological triplicates, and error bars represent standard deviation. (C) GC−MS total ion traces of culture supernatants of the Δ*ipdE1*, Δ*ipdE4*, and Δ*ipdE2* strains incubated with cholesterol. The peak corresponding to TMS-derivatized 5-OH-HIP is labeled. "ISTD" indicates the peak corresponds to 5α-cholestane, the internal standard. Cholesterol-derived metabolites were extracted and derivatized as described in Materials and Methods.

$NaHPO_4$, 500 mM NaCl, pH 7.4. Fractions that contained IpdE1-IpdE2, as assessed by SDS-PAGE and spectrophotometric analysis, were pooled, concentrated, and loaded onto a Superdex 200 16/60 column equilibrated with 20 mM Tris-HCl, 200 mM NaCl, pH 8.0 and operated at a flow rate of 1 mL/min. IpdE1-IpdE2 containing fractions were identified by SDS-PAGE. Protein was concentrated to ∼25 mg/mL and flash-frozen for storage.

Determination of FAD Content. The concentration of intact IpdE1-IpdE2 was measured by UV. A known amount of IpdE1-IpdE2, as determined by absorbance at 280 nm (ε = 214,740 μM^{-1} cm^{-1}, calculated by primary sequence analysis via the Swiss Institute of Bioinformatics ProtParam tool), was denatured with 8 M urea. Subsequently, the denatured protein was removed by centrifugation for 10 min at 18,000*g*. The resulting supernatant was collected, and the concentration of FAD was measured by absorbance at 260 nm (ε = 11,300 μM^{-1} cm^{-1}). The protein/free FAD concentration ratio was then determined. UV−vis spectroscopy was performed with a UV-2550 spectrophotometer (Shimadzu).

IpdE1-IpdE2 Activity Assay and MALDI-TOF Analysis. Substrate (50 μM) and ferrocenium hexafluorophosphate (250 μM) were incubated in 100 mM TAPS, pH 8.5, at 25 °C. The reaction was initiated by the addition of 1−100 nM enzyme and monitored spectroscopically at 300 nm (ε = 4.3 mM^{-1} cm^{-1}).[43] 5OH-HIP-CoA, octanoyl-CoA, dihydroferuloyl-CoA, and 3-oxo-4-pregnene-20-carboxyl-CoA were used as substrates. Initial velocities were obtained for the first 10−15% of the reaction.

For MALDI-TOF analysis, IpdE1-IpdE2 (50 nM) was incubated with 50 μM 5OH-HIP-CoA and 1 mM ferrocenium hexafluorophosphate, in 100 mM TAPS, pH 8.5, at 25 °C for 30 and 60 min. The reaction was stopped by the addition of 3% TFA, and loaded onto a C18 ZipTip column, washed with 0.1% TFA, and eluted with 50% acetonitrile containing 0.1% TFA. Purified products were mixed 1:1 with 2,5-dihydroxybenzoic acid matrix and spotted onto an MTP384 target plate

https://dx.doi.org/10.1021/acs.biochem.0c00005
Biochemistry 2020, 59, 1113−1123

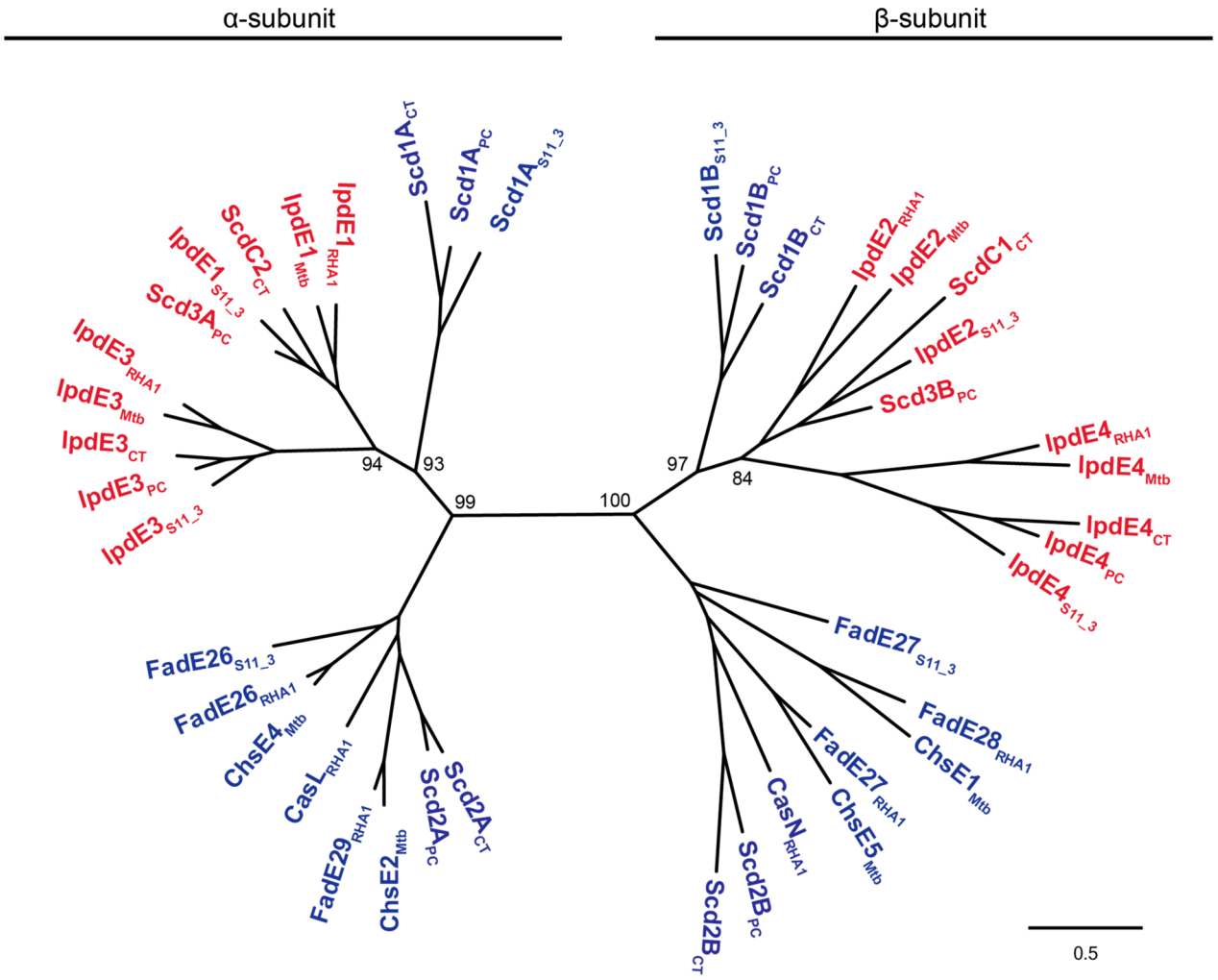

Figure 4. Phylogenetic analysis of the subunits of $\alpha_2\beta_2$ACADs from steroid-degrading bacteria. Sequences of the α- and β-subunits of 21 ACADs were retrieved from the following steroid-degrading bacteria identified using subscripts: Mtb, Mtb H37rv; RHA1, *R. jostii* RHA1; CT, *C. testosteroni* CNB-2; PC, *Pseudomonas* sp. Chol1; S11_3, *Cellvibrionales* sp. S11_3. Sequences were aligned, curated, and clustered as described. α- and β-subunit clusters are located on the left and right lobe of the tree, respectively. Enzymes involved in side-chain and ring C/D degradation are highlighted in blue and red, respectively. The scale bar represent substitutions per site.

for analysis by matrix-assisted laser desorption time-of-flight mass spectrometry (MALDI-TOF MS) on an Autoflex II TOF/TOF instrument (Bruker) operating in negative reflectron mode. An MTP384 ground-steel target plate (Bruker) was used for the acquisition of MALDI-TOF mass spectra. Matrices for MALDI-TOF MS were prepared by dissolving 2,5-dihydroxybenzoic acid (20 mg/mL) in a 7:3 (v/v) mixture of 0.1% (v/v) TFA/acetonitrile. MALDI-TOF spectra were analyzed with Bruker FlexAnalysis 3.0 software.

Characterization of 5OH-HIP-CoA Reaction Products by ^{1}H NMR Spectroscopy. 5-OH-HIPE-CoA was synthesized by incubating 100 μM 5-OH-HIP-CoA, 200 μM ferrocenium hexafluorophosphate, and 10 μM IpdE1-IpdE2 in 100 mM TAPS buffer at pH 8.5 for 1 h. The resulting product was purified by HPLC on a C18 column using 10 mM ammonium acetate with a linear gradient of acetonitrile from 5% to 100% over 50 min. ^{1}H NMR spectra of 5-OH-HIP-CoA and 5-OH-HIPE-CoA were obtained on a 700 MHz Bruker spectrometer by dissolving the CoA esters in D_2O to a final concentration of 50 μM. Chemical shifts are reported in ppm (δ) calibrated using residual protic solvent as an internal reference.

SAXS Analysis. SAXS profiles of proteins at three concentrations (4.5, 2.25, and 1.125 mg/mL) were collected at the 16 LiX beamline of the National Synchrotron Light Source II (Brookhaven National Laboratory), which has an energy of 6−18 keV during normal operation. The scattering contribution of the protein complex was determined by subtracting the background scattering of the buffer. The one-dimensional SAXS profiles were used to generate a three-dimensional *ab initio* model of IpdE1-IpdE2 with the ATSAS software suite.[44] Briefly, the one-dimensional SAXS profiles were averaged to generate a well-behaved P(r) curve, which was input into DAMMIF to generate 10 protein-shaped bead models. The bead models were compared in DAMSEL, and the most probable model was selected and then compared with the crystal structure of ChsE4-ChsE5 (PDB: 4X28) by means of the CRYSOL program.

RESULTS

Gene Synteny of ipdE1 and ipdE2 Orthologs. The *ipdE1* and *ipdE2* genes are among 13 genes that encode HIP catabolism enzymes in characterized steroid-degrading bacteria. We had previously noted that although these two genes

https://dx.doi.org/10.1021/acs.biochem.0c00005
Biochemistry 2020, 59, 1113−1123

occur in divergently transcribed operons in *Mtb* and *R. jostii* RHA1, they occur in the same operon in some Gram-negative bacteria.[10] Given the diversity of genomic arrangements for *ipdE1* (*fadE30*) and *ipdE2* (*fadE33*), we examined whether genes annotated as *fadE30* or *fadE33* in bacterial genomes were true orthologs of *ipdE1* and *ipdE2* using OrthologueDB (Figure S1A), a reciprocal BLAST-based algorithm used to ensure the validity of the orthologous sequences.[45] Based on the pairwise distances between aligned sequences, *ipdE1* and *ipdE2* are clearly distinct α-and β-subunit family members, respectively, of the heterotetrameric FadE protein family that, interestingly, occur in a variety of possible operonic arrangements (Figure S1B).

To further investigate the co-occurrence of the *ipdE1*, *ipdE2*, *ipdE3*, and *ipdE4* genes, we studied their genomic arrangement in other bacteria. Briefly, we performed a Multigene BLAST using the sequences of the *Mtb* IpdE proteins in architecture search mode against the GenBank BCT database. This analysis indicates that the HIP-degrading ACAD genes are syntenic in mycolic acid-producing Actinobacteria, with *ipdE1* and *ipdE3-ipdE4-ipdE2* located in adjacent, divergently transcribed operons (Figure 2). Further, a different synteny is conserved in Proteobacteria, with *ipdE1-ipdE2* and *ipdE3-ipdE4* forming adjacent pairs. In Actinobacteria that do not produce mycolic acids, the four *ipdE* genes occur in up to three predicted operons, as exemplified by *Kibdelosporangium phytohabitans* (Figure 2). Nevertheless, *ipdE3* and *ipdE4* orthologs consistently occurred adjacent to each other. These analyses indicate a variety of potential operonic arrangements for the α-subunit *ipdE1* and β-subunit *ipdE2* ACAD genes across Actinobacteria and Proteobacteria.

Deletion of ipdE1 and ipdE2. To investigate the role of *ipdE1* and *ipdE2* in mycobacteria, we used recombineering to replace each gene in *M. smegmatis* with an antibiotic resistance cassette (Figure S2). The two deletion strains had similar phenotypes, growing at ∼75% the rate of wild-type *M. smegmatis* on cholesterol and to ∼40% the yield of biomass (Figure 3). By contrast, the mutant strains grew normally on glycerol. These phenotypes are similar to those of Δ*fadD3*[23] and Δ*ipdE4* mutants,[10] which are disrupted in their ability to catabolize the rings C/D of cholesterol. Interestingly, neither mutant displayed the cholesterol-dependent toxicity observed in other KstR2-regulon mutants, such as Δ*ipdAB* and Δ*echA20*.[10,46]

To further probe the biochemical function of IpdE1 and IpdE2, we investigated the transformation of cholesterol by the mutant strains. In these experiments, cell suspensions were incubated with cholesterol, and GC−MS was used to detect and characterize any metabolites that accumulated in the supernatant. In these assays, the Δ*ipdE1* and Δ*ipdE2* mutants transformed cholesterol to 5-OH-HIP and trace amounts of the 5-OH-HIP lactone (HIL) (Figure 3C, Figures S3 and S4). These metabolites were not detected when the Δ*ipdE4* strain was used.

A transposon disruption mutant of *ipdE2* in *Mtb* had a similar phenotype as the Δ*ipdE1* and Δ*ipdE2* mutants of *M. smegmatis*. Thus, when *Mtb* CDC1551 *ipdE2*::Tn was grown on cholesterol, analysis of the culture supernatant using mass spectrometry revealed the accumulation of 5-OH-HIP lactone (HIL; Figure S5).

Bioinformatic Evidence for an IpdE1-IpdE2 Heterocomplex. On the basis of the essentially identical phenotypes of the Δ*ipdE1* and Δ*ipdE2* mutants, we hypothesized that their gene products form a heterocomplex analogous to characterized $\alpha_2\beta_2$ ACADs such as ChsE4-ChsE5 and ChsE1-ChsE2.[26,27] To investigate this hypothesis, we conducted a phylogenetic analysis of the subunits of characterized $\alpha_2\beta_2$ ACADs and their homologues in diverse steroid-degrading bacteria: two Actinobacteria and three Proteobacteria. Homologues fulfilled two criteria: (a) their genes co-occurred with known steroid catabolic genes; (b) they were reciprocal best hits with characterized $\alpha_2\beta_2$ ACADs. Sequences (Table S3) were collected from six pathways in the five strains: the cholesterol catabolic pathways of *Mtb* H37Rv, *R. jostii* RHA1, and *Cellvibrionales* sp. S11_3, a recently discovered cholesterol-degrading proteobacterium isolated from a marine sponge;[1] and the cholate catabolic pathways of *R. jostii* RHA1, *Comamonas testosteroni* CNB-2, and *Pseudomonas* sp. Chol1. Sequences were aligned, edited to remove gaps in the alignment, then clustered using maximum-likelihood. The resulting tree (Figure 4) is characterized by two well-separated lobes comprising the α- and β-subunits, respectively, of the ACADs. Within each lobe of the tree, the sequences further clustered largely according to the enzymes' substrate specificities. Notably, the sequences originating from HIP-degrading enzymes form well-defined clusters. The clustering of IpdE1 and IpdE2 with the α- and β-subunits, respectively, supports the hypothesis that IpdE1-IpdE2 is an $\alpha_2\beta_2$ ACAD.

To further explore the relationship of IpdE1 and IpdE2 with characterized $\alpha_2\beta_2$ ACADs, the amino acid sequence alignment of $IpdE1_{Mtb}$, $IpdE2_{Mtb}$, ChsE4-ChsE5, and ChsE1-ChsE2 were inspected for conserved motifs (Figure 5).[26,27] Importantly,

Figure 5. Conserved residues in IpdE proteins and characterized *Mtb*$\alpha_2\beta_2$ ACADs. Alignment of the amino acid sequences of IpdE1, IpdE2, IpdE3, and IpdE4 from *Mtb* with those of ChsE4-ChsE5 and ChsE1-ChsE2. Conserved residues that participate in FAD binding are highlighted in green. The conserved catalytic base is highlighted in magenta and denoted with an asterisk.

IpdE1 and IpdE2 shared key residues that are conserved in the characterized $\alpha_2\beta_2$ ACADs. This includes the FAD-binding residues found in ChsE4-ChsE5 and ChsE1-ChsE2 as well as the catalytic glutamate of the α subunit (Glu244 in IpdE1).

Production and Purification of an IpdE1-IpdE2 $\alpha_2\beta_2$ Heterotetramer. Initial attempts to express *ipdE1* and *ipdE2* in *E. coli*, either individually or coexpressed on separate plasmids, did not yield soluble protein. Based on our success in heterologously producing mycobacterial proteins in *R. jostii*

https://dx.doi.org/10.1021/acs.biochem.0c00005
Biochemistry 2020, 59, 1113−1123

RHA1,[47] we cloned *ipdE1* and *ipdE2* into pTip, a thiostrepton-inducible expression vector for *Rhodococcus*. When each protein was produced separately with N-terminal His-tags, most was insoluble (Figure S6). Other ACADs were produced as soluble heterocomplexes when the two genes were coexpressed in *E. coli*.[27] Accordingly, we developed a dual expression vector to coexpress *ipdE1* and *ipdE2* in *R. jostii* RHA1. Briefly, we inserted a second thiostrepton-inducible expression cassette into a neutral site in pTip. Using this strategy, a vector containing two inducible expression cassettes, for *ipdE1* and N-terminally His_6-tagged *ipdE2*, respectively, was created. This vector allowed for coexpression of *ipdE1* and *His_6-ipdE2* in *R. jostii* RHA1 and yielded a stable, soluble protein complex that could be isolated by IMAC. SDS-PAGE analysis indicated that the purified complex (IpdE1-IpdE2 hereafter) was composed of a ~1:1 ratio of IpdE1/IpdE2 subunits (Figure S7). The stoichiometry was confirmed by size exclusion chromatography, revealing a single species corresponding to a molecular weight of approximately 154 kDa, consistent with an $\alpha_2\beta_2$ tetrameric protein complex comprising IpdE1 (43 kDa) and IpdE2 (34 kDa) (Figure S8). The identities of IpdE1 and IpdE2 were confirmed by tryptic digestion and MALDI-TOF MS. The UV−vis spectrum of the purified complex revealed absorbance maxima at 370 and 446 nm, consistent with a FAD cofactor (Figure S9), and was found to contain 1.59 ± 0.04 FAD molecules bound to each $\alpha_2\beta_2$ protein complex, similar to other $\alpha_2\beta_2$ heterotetramers which bind two FAD molecules per complex,[27] although sometimes isolated with incomplete occupancy.

Transformation of 5-OH-HIP-CoA by IpdE1-IpdE2. On the basis of our metabolite analysis of *ipdE1* and *ipdE2* knockout strains, we hypothesized the IpdE1-IpdE2 complex converts 5OH-HIP-CoA to 5OH-HIPE-CoA. To test this hypothesis, IpdE1-IpdE2 was incubated with 5OH-HIP-CoA and the resulting reaction products analyzed by mass spec. The mass spectra indicated that the 5-OH-HIP-CoA had been completely converted to 5-OH-HIPE-CoA, specified by a −2 shift in m/z, representing a loss of two hydrogens (Figure 6A)per. Interestingly, an IpdE3-IpdE2 heterocomplex previously purified from *E. coli*,[27] did not oxidize 5-OH-HIP-CoA (Figure 6B), suggesting that only the IpdE1-IpdE2 complex is required for 5-OH-HIP-CoA conversion to 5OH-HIPE-CoA.

Subsequently, we examined the substrate preference of IpdE1-IpdE2 with four acyl-CoA esters: 5-OH-HIP-CoA, octanoyl-CoA, dihydroferuloyl-CoA, and 3-oxo-4-pregnene-20-carboxyl-CoA (3-OPC-CoA) (Figure S10). At 25 °C and 50 μM substrate, IpdE1-IpdE2 preferred 5-OH-HIP-CoA with a specific activity of 41 ± 12 μmol/min/mg, compared to 1.6 ± 0.7 μmol/min/mg with octanoyl-CoA as substrate, 0.3 ± 0.2 μmol/min/mg, with dihydroferuloyl-CoA as substrate, and no activity with 3-OPC-CoA.

Analysis by ^{1}H NMR spectroscopy confirmed that IpdE1-IpdE2 catalyzes the oxidation of 5OH-HIP-CoA to 5OH-HIPE-CoA. A comparison of the ^{1}H NMR spectra of 5OH-HIP-CoA before and after incubation with IpdE1-IpdE2 reveals the appearance of peaks at δ 6.90 and 6.31, which correspond to the H10 and H11 alkene protons, respectively, of 5OH-HIPE-CoA (Figure 7).

Structural Similarities between IpdE1-IpdE2 and ChsE4-ChsE5 Are Revealed by SAXS Analysis. To obtain a nanometer-scale structural envelope for the IpdE1-IpdE2 complex in the solution state, we acquired its SAXS profile and constructed a three-dimensional *ab initio* envelope. IpdE1-IpdE2 shares about 30% amino acid sequence identity with ChsE4-ChsE5, an $\alpha_2\beta_2$ ACAD involved in cholesterol side change degradation.[28] Given their other experimental relationships, we hypothesized that the two enzymes have similar structures. The X-ray scattering profile of the ChsE4-ChsE5 crystal structure is similar in shape with the scattering profile of IpdE1-IpdE2, and oscillations of the two profiles occur around the same q value (Figure 8A). The radius of the IpdE1-IpdE2 complex was determined to be about 38 Å, whereas that of the ChsE4-ChsE5 complex is about 36 Å. The three-dimensional envelope of IpdE1-IpdE2 in the solution state was superimposed onto the crystal structure of ChsE4-ChsE5 (Figure 8B). The two-sphere models share highly similar shapes.

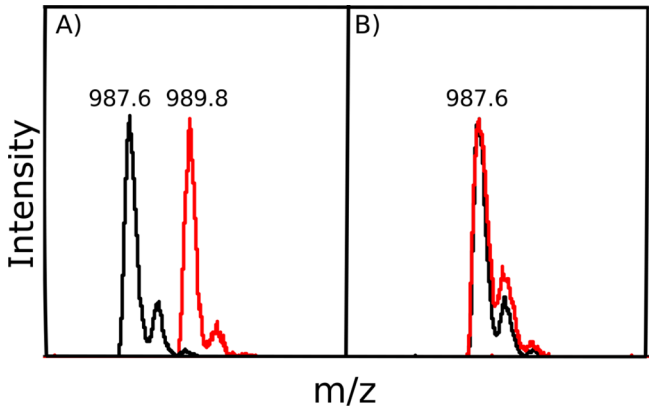

Figure 6. IpdE1-IpdE2 catalyzes the dehydrogenation of 5OH-HIPCoA, but IpdE3-IpdE2 does not. After incubation of the enzyme and substrate at 25 °C for 30 or 60 min, samples of the reaction mixture were combined with 2,5-dihydroxybenzoic acid matrix (1:1, v/v), and MALDI-TOF spectral data were collected in negative reflectron mode. (A) IpdE1-IpdE2 catalyzed the dehydrogenation of 5OH-HIP-CoA (m/z = 989.8) to 5OH-HIPE-CoA (m/z = 987.6) after 30 min. Traces at 0 min (red) and 30 min (black). (B) IpdE3-IpdE2 did not catalyze the dehydrogenation of 5OH-HIP-CoA. Traces at 0 min (red) and 60 min (black).

DISCUSSION

This study establishes that IpdE1-IpdE2 is an $\alpha_2\beta_2$ heterotetrameric ACAD that catalyzes the dehydrogenation of 5OH-HIP-CoA to (*E*)-5OH-HIPE-CoA. The deletion of either gene in *M. smegmatis* or disruption of *ipdE1* in *Mtb* yielded mutants that accumulated 5-OH HIP in the culture supernatant when incubated with cholesterol. Moreover, IpdE1-IpdE2 from *Mtb*, heterologously produced in *R. jostii* RHA1, catalyzed the dehydrogenation of 5OH-HIP-CoA to (*E*)-5OH-HIPE-CoA as confirmed by MALDI-TOF MS and ^{1}H NMR spectroscopy. The specific activity of IpdE1-IpdE2 for the dehydrogenation of 5OH-HIP-CoA is 25-fold higher than for a simple fatty acyl-CoA. Dehydrogenation of a ring-intact substrate 3-oxo-4-pregnene-20-carboxyl-CoA, a metabolite formed in the KstR-regulated arm of the cholesterol catabolism pathway, is not detectably catalyzed by IpdE1-IpdE2, and an aromatic substrate is a very poor substrate. The heterotetrameric structure of IpdE1-IpdE2 was confirmed by gel filtration chromatography and small-angle X-ray scattering. These results extend the molecular genetic analyses reported in *C. testosteroni* TA441.[32] Taken together, this work identifies the enzyme that catalyzes the initial step in the β-oxidative pathway that leads to degradation of steroid C and D rings.

https://dx.doi.org/10.1021/acs.biochem.0c00005
Biochemistry 2020, 59, 1113−1123

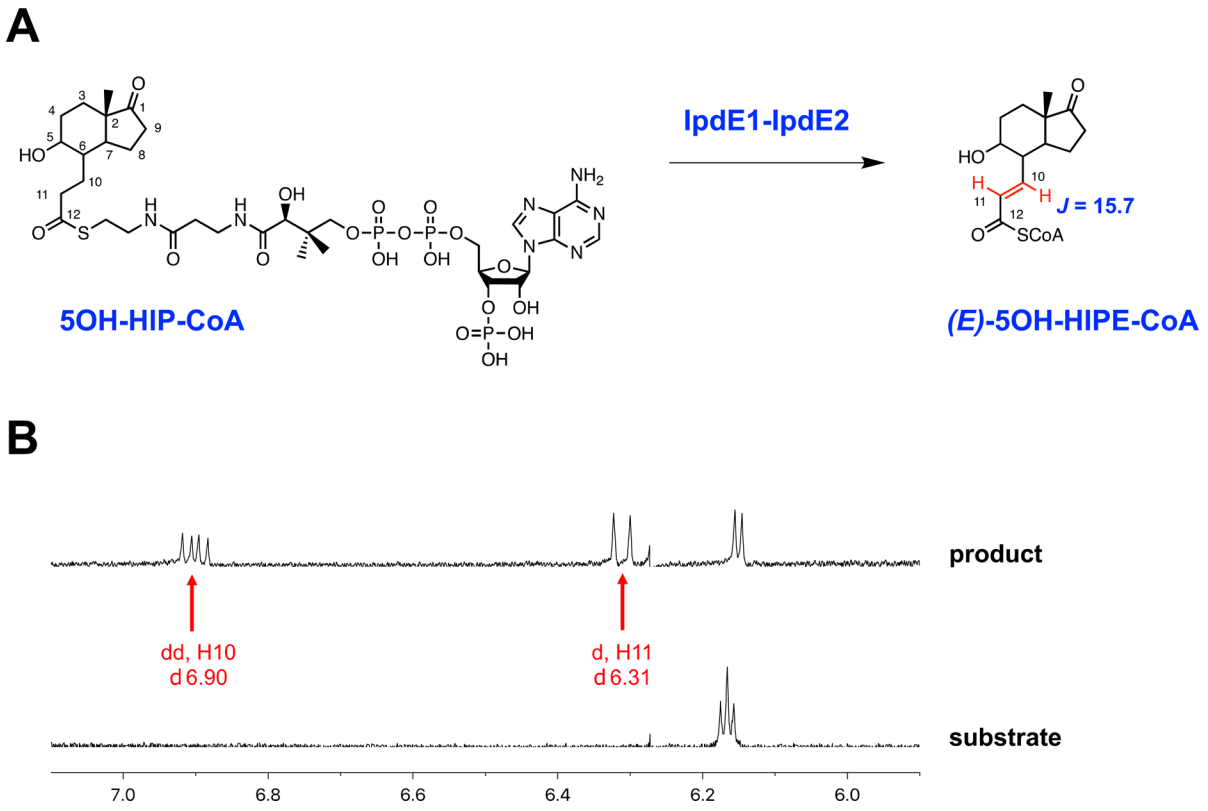

Figure 7. IpdE1-IpdE2 catalyzes the formation of (*E*)-5OH-HIPE-CoA. (A) Structures of 5OH-HIP-CoA (substrate) and (*E*)-5OH-HIPE-CoA (product). (B) ^{1}H NMR spectra of the IpdE1-IpdE2 reaction mixture (700 MHz), highlighting the changes in the alkene region: H10, J = 15.7; H11, J = 15.7.

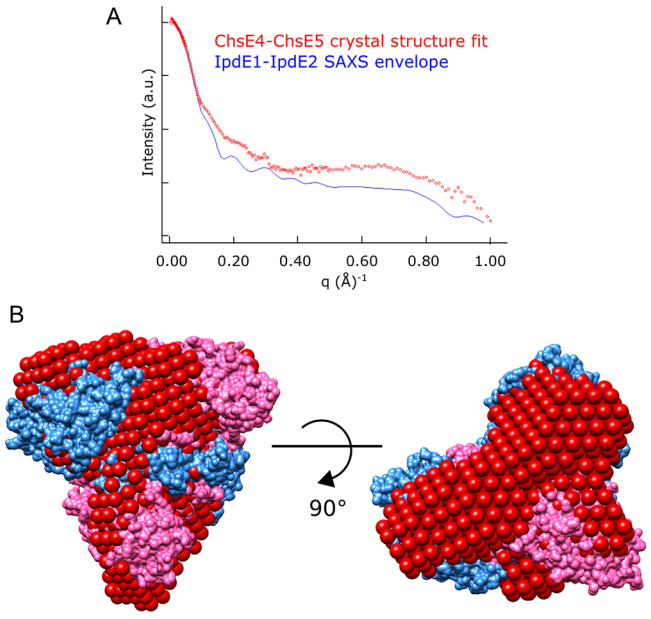

Figure 8. IpdE1-IpdE2 structural characterization by SAXS. (A) The theoretical scattering profile of the ChsE4-ChsE5 crystal structure, defined as scattering intensity, versus the experimentally determined scattering profile for IpdE1-IpdE2 in solution. (B) The *ab initio* envelope of IpdE1-IpdE2, represented by the red spheres, was superimposed over the crystal structure of ChsE4-ChsE5 (PDB: 4X28). ChsE4 is labeled in blue, and ChsE5 is labeled in pink.

IpdE1-IpdE2 is typical of the $\alpha_2\beta_2$ ACADs involved in cholesterol side-chain degradation, such as ChsE1-ChsE2 and ChsE4-ChsE5. A defining feature of the characterized $\alpha_2\beta_2$ ACADs is that they harbor two FAD molecules per tetramer.[27,28,48] The FAD content of IpdE1-IpdE2 is consistent with this stoichiometry. Moreover, sequence analyses revealed that IpdE1 and IpdE2 contain the FAD-binding residues characteristic of the α- and β-subunits, respectively (Figure 5). IpdE1 also contains Glu244, the conserved residue of the α subunit that acts as the catalytic base in other $\alpha_2\beta_2$ ACADs. Thus, IpdE1-IpdE2 contains all of the conserved residues required to form two active sites, one at each α/β interface, as occurs in other $\alpha_2\beta_2$ ACADs.

Given that IpdE1-IpdE2 is a typical $\alpha_2\beta_2$ ACAD, it is unclear why the *ipdE1* and *ipdE2* genes are not adjacent to each other in Actinobacteria chromosomes. This arrangement is contrary to most pairs of *ipdE* genes that encode these enzymes, including *ipdE1* and *ipdE2* in steroid-degrading proteobacteria. One exception is *casL* and *casN*, predicted to encode an $\alpha_2\beta_2$ ACAD involved in cholate side-chain degradation.[9] However, these genes are separated by a single gene and are located in the same operon. Overall, there is a surprising degree of variation of the order and organization of *ipdE* genes in Actinobacteria considering that the *ipdE1* and *ipdE2* gene products are required in equimolar amounts.

The growth of the Δ*ipdE1* and Δ*ipdE2* mutants on cholesterol is consistent with the ability of these mutants to grow on the side chain and a portion of the steroid rings. Nevertheless, the viability of the different HIP catabolic mutants varies considerably with some showing a cholesterol-dependent toxicity.[10] Thus, Δ*fadD3* mutants grow on cholesterol at the same rate as the wild-type strain, while Δ*ipdAB* mutants do not grow on cholesterol at all.[10,49] The

https://dx.doi.org/10.1021/acs.biochem.0c00005
Biochemistry 2020, 59, 1113−1123

inability to grow on cholesterol has been associated with the accumulation of HIP-derived CoA thioesters and the concomitant depletion of CoASH in the cell.[10] The phenotype of the Δ*ipdE1* and Δ*ipdE2* mutants is similar to that of the Δ*ipdE4* mutant: on cholesterol, these grow more slowly than the Δ*fadD3* mutant and accumulate an acid in the culture medium that is presumed to correspond to the acyl moiety of the ablated enzyme's CoA substrate. The correlation between the growth rates of the HIP catabolic mutants and the intracellular levels of free CoASH is currently being investigated.

In conclusion, the functional and structural characterization of IpdE1-IpdE2 expands the range of known $\alpha_2\beta_2$ ACADs. This provides important insight into the first step in the β-oxidative degradation of steroid C and D rings that occurs in *Mtb* and all known steroid-degrading bacteria. In addition, this study establishes that the $\alpha_2\beta_2$ ACADs characteristic of bacterial steroid catabolic pathways do not have to be encoded by adjacent cistronic genes.

■ ASSOCIATED CONTENT

Supporting Information

The Supporting Information is available free of charge at https://pubs.acs.org/doi/10.1021/acs.biochem.0c00005.

> Additional information on oligonucleotide constructs, a heat map of ACAD orthologs, metabolomic profiles of *M. smegmatis ipdE* mutants, the metabolomic profile of *Mtb ipdE2* mutants, IpdE1-IpdE2 protein expression, size-exclusion chromatograms, SDS-PAGE data, UV−vis profiles, and chemical structures of substrates in the enzyme activity assay (PDF)

Accession Codes

UniProt accession IDs for proteins used in this work are as follows: IpdE1 (FadE30), I6Y3V5; IpdE2 (FadE33), I6YCF5; IpdE3 (FadE31), I6YGH7; IpdE4 (FadE32), P96845.

■ AUTHOR INFORMATION

Corresponding Authors

Lindsay D. Eltis − *Department of Microbiology and Immunology and Department of Biochemistry and Molecular Biology, The University of British Columbia, Vancouver, British Columbia V6T 1Z3, Canada;* orcid.org/0000-0002-6774-8158; Phone: +1-604-822-0042; Email: leltis@mail.ubc.ca; Fax: +1-604-822-6041

Nicole S. Sampson − *Department of Chemistry, Stony Brook University, Stony Brook, New York 11794-3400, United States;* orcid.org/0000-0002-2835-7760; Phone: +1-631-632-7952; Email: nicole.sampson@stonybrook.edu; Fax: +1-631-632-5738

Authors

John E. Gadbery − *Department of Chemistry, Stony Brook University, Stony Brook, New York 11794-3400, United States;* orcid.org/0000-0002-8998-2658

James W. Round − *Department of Microbiology and Immunology, The University of British Columbia, Vancouver, British Columbia V6T 1Z3, Canada*

Tianao Yuan − *Department of Chemistry, Stony Brook University, Stony Brook, New York 11794-3400, United States;* orcid.org/0000-0002-4700-8654

Matthew F. Wipperman − *Department of Chemistry, Stony Brook University, Stony Brook, New York 11794-3400, United States; Immunology Program, Memorial Sloan Kettering Cancer Center, New York, New York 10065, United States; Clinical & Translational Science Center, Weill Cornell Medicine, New York, New York 10065, United States;* orcid.org/0000-0003-1436-3366

Keith T. Story − *Department of Biochemistry and Molecular Biology, The University of British Columbia, Vancouver, British Columbia V6T 1Z3, Canada*

Adam M. Crowe − *Department of Biochemistry and Molecular Biology, The University of British Columbia, Vancouver, British Columbia V6T 1Z3, Canada;* orcid.org/0000-0002-5487-2520

[#]Israel Casabon − *Department of Microbiology and Immunology, The University of British Columbia, Vancouver, British Columbia V6T 1Z3, Canada*

Jie Liu − *Department of Microbiology and Immunology, The University of British Columbia, Vancouver, British Columbia V6T 1Z3, Canada*

Xinxin Yang − *Department of Chemistry, Stony Brook University, Stony Brook, New York 11794-3400, United States;* orcid.org/0000-0002-5162-5030

Complete contact information is available at: https://pubs.acs.org/10.1021/acs.biochem.0c00005

Funding

This research is funded by an NIH grant (RO1AI134054) to N.S.S. and an Operating Grant from the Canadian Institutes for Health Research (CIHR) to L.D.E. M.F.W. acknowledges support from the National Center for Advancing Translational Sciences of the NIH (TL1TR002386). A.M.C. was supported by a CIHR doctoral fellowship. L.D.E. is the recipient of a Canada Research Chair. Beamline LiX is supported primarily by the National Institutes of Health (NIH), National Institute of General Medical Sciences (NIGMS), through a Biomedical Technology Research Resource P41 grant (P41GM111244) and by the DOE Office of Biological and Environmental Research (KP1605010).

Notes

The authors declare no competing financial interest.

[#]I.C. is deceased.

■ ACKNOWLEDGMENTS

The SAXS experiments were conducted using resources of the National Synchrotron Light Source II, a U.S. Department of Energy (DOE) Office of Science User Facility operated for the DOE Office of Science by Brookhaven National Laboratory under contract no. DE-SC0012704. We thank Xiaoxi Yu and Surita Bhatia for the IpdE1-IpdE2 SAXS data collection. Dr. Tomohiro Tamura provided the pTipQC2 vector. The *Mtb CDC1551 ipdE2*::Tn mutant was obtained from BEI Resources, NIAID, NIH.

■ REFERENCES

(1) Holert, J., Cardenas, E., Bergstrand, L. H., Zaikova, E., Hahn, A. S., Hallam, S. J., and Mohn, W. W. (2018) Metagenomes reveal global distribution of bacterial steroid catabolism in natural, engineered, and host environments. *mBio 9* (1), 1.

(2) Donova, M. V., and Egorova, O. V. (2012) Microbial steroid transformations: current state and prospects. *Appl. Microbiol. Biotechnol. 94* (6), 1423−1447.

(3) Van der Geize, R., Yam, K., Heuser, T., Wilbrink, M. H., Hara, H., Anderton, M. C., Sim, E., Dijkhuizen, L., Davies, J. E., Mohn, W. W., and Eltis, L. D. (2007) A gene cluster encoding cholesterol

catabolism in a soil actinomycete provides insight into *Mycobacterium tuberculosis* survival in macrophages. *Proc. Natl. Acad. Sci. U. S. A. 104* (6), 1947−1952.
(4) Pandey, A. K., and Sassetti, C. M. (2008) Mycobacterial persistence requires the utilization of host cholesterol. *Proc. Natl. Acad. Sci. U. S. A. 105* (11), 4376−4380.
(5) Organization, W. H. (2017) WHO "Global Tuberculosis Report 2016, http://www.who.int/tb/publications/global_report/en/.
(6) VanderVen, B. C., Fahey, R. J., Lee, W., Liu, Y., Abramovitch, R. B., Russell, D. G., Memmott, C., Perola, E., Deininger, D. D., Wang, T., Locher, C. P., Crowe, A. M., and Eltis, L. D. (2015) Novel inhibitors of cholesterol degradation in *Mycobacterium tuberculosis* reveal how the bacterium's metabolism is constrained by the intracellular environment. *PLoS Pathog. 11* (2), No. e1004679.
(7) Yuan, T., and Sampson, N. S. (2018) Hit generation in TB drug discovery: from genome to granuloma. *Chem. Rev. 118* (4), 1887−1916.
(8) Horinouchi, M., Hayashi, T., and Kudo, T. (2012) Steroid degradation in *Comamonas testosteroni*. *J. Steroid Biochem. Mol. Biol. 129* (1−2), 4−14.
(9) Mohn, W. W., Wilbrink, M. H., Casabon, I., Stewart, G. R., Liu, J., van der Geize, R., and Eltis, L. D. (2012) Gene cluster encoding cholate catabolism in *Rhodococcus spp*. *J. Bacteriol. 194* (24), 6712−6719.
(10) Crowe, A. M., Casabon, I., Brown, K. L., Liu, J., Lian, J., Rogalski, J. C., Hurst, T. E., Snieckus, V., Foster, L. J., and Eltis, L. D. (2017) Catabolism of the last two steroid rings in *Mycobacterium tuberculosis* and other bacteria. *mBio 8* (2), 1.
(11) Thomas, S. T., VanderVen, B. C., Sherman, D. R., Russell, D. G., and Sampson, N. S. (2011) Pathway profiling in *Mycobacterium tuberculosis*: elucidation of cholesterol-derived catabolite and enzymes that catalyze its metabolism. *J. Biol. Chem. 286* (51), 43668−43678.
(12) Martin, C. K. A. (1977) Microbial cleavage of sterol side chains. *Adv. Appl. Microbiol. 22*, 29−58.
(13) McLean, K. J., Lafite, P., Levy, C., Cheesman, M. R., Mast, N., Pikuleva, I. A., Leys, D., and Munro, A. W. (2009) The structure of *Mycobacterium tuberculosis* CYP125: Molecular basis for cholesterol binding in a P450 needed for host infection. *J. Biol. Chem. 284*, 35524−35533.
(14) Driscoll, M. D., McLean, K. J., Levy, C., Mast, N., Pikuleva, I. A., Lafite, P., Rigby, S. E., Leys, D., and Munro, A. W. (2010) Structural and biochemical characterization of *Mycobacterium tuberculosis* CYP142: evidence for multiple cholesterol 27-hydroxylase activities in a human pathogen. *J. Biol. Chem. 285* (49), 38270−38282.
(15) Nesbitt, N. M., Yang, X., Fontan, P., Kolesnikova, I., Smith, I., Sampson, N. S., and Dubnau, E. (2010) A thiolase of *Mycobacteriumtuberculosis* is required for virulence and production of androstenedione and androstadienedione from cholesterol. *Infect. Immun. 78* (1), 275−282.
(16) Yuan, T., Yang, M., Gehring, K., and Sampson, N. S. (2019) *Mycobacterium tuberculosis* exploits a heterohexameric enoyl-CoA hydratase retro-aldolase complex for cholesterol catabolism. *Biochemistry 58* (41), 4224−4235.
(17) Gibson, D. T., Wang, K. C., Sih, C. J., and Whitlock, H., Jr. (1966) Mechanisms of steroid oxidation by microorganisms. IX. On the mechanism of ring A cleavage in the degradation of 9, 10-seco steroids by microorganisms. *J. Biol. Chem. 241* (3), 551−559.
(18) Horinouchi, M., Yamamoto, T., Taguchi, K., Arai, H., and Kudo, T. (2001) Meta-cleavage enzyme gene *tesB* is necessary for testosterone degradation in *Comamonas testosteroni* TA441. *Microbiology 147* (12), 3367−3375.
(19) van der Geize, R., Hessels, G. I., van Gerwen, R., van der Meijden, P., and Dijkhuizen, L. (2002) Molecular and functional characterization of *kshA* and *kshB*, encoding two components of 3-ketosteroid 9alpha-hydroxylase, a class IA monooxygenase, in *Rhodococcuserythropolis* strain SQ1. *Mol. Microbiol. 45* (4), 1007−1018.
(20) Kendall, S. L., Burgess, P., Balhana, R., Withers, M., Ten Bokum, A., Lott, J. S., Gao, C., Uhia-Castro, I., and Stoker, N. G. (2010) Cholesterol utilization in mycobacteria is controlled by two TetR-type transcriptional regulators: KstR and KstR2. *Microbiology 156* (5), 1362−1371.
(21) Capyk, J. K., Casabon, I., Gruninger, R., Strynadka, N. C., and Eltis, L. D. (2011) Activity of 3-ketosteroid 9a-hydroxylase (KshAB) indicates cholesterol side chain and ring degradation occur simultaneously in *Mycobacterium tuberculosis*. *J. Biol. Chem. 286* (47), 40717−40724.
(22) Lee, S. S., and Sih, C. J. (1967) Mechanisms of steroid oxidation by microorganisms. XII. metabolism of hexahydroindan-propionic acid derivatives*. *Biochemistry 6* (5), 1395−1403.
(23) Casabon, I., Crowe, A. M., Liu, J., and Eltis, L. D. (2013) FadD3 is an acyl-CoA synthetase that initiates catabolism of cholesterol rings C and D in actinobacteria. *Mol. Microbiol. 87* (2), 269−283.
(24) Casabon, I., Zhu, S. H., Otani, H., Liu, J., Mohn, W. W., and Eltis, L. D. (2013) Regulation of the KstR2 regulon of *Mycobacterium tuberculosis* by a cholesterol catabolite. *Mol. Microbiol. 89* (6), 1201−1212.
(25) Ghisla, S., and Thorpe, C. (2004) Acyl-CoA dehydrogenases. A mechanistic overview. *Eur. J. Biochem. 271* (3), 494−508.
(26) Thomas, S. T., and Sampson, N. S. (2013) *Mycobacterium tuberculosis* utilizes a unique heterotetrameric structure for dehydrogenation of the cholesterol side chain. *Biochemistry 52* (17), 2895−2904.
(27) Wipperman, M. F., Yang, M., Thomas, S. T., and Sampson, N. S. (2013) Shrinking the FadE proteome of *Mycobacteriumtuberculosis*: insights into cholesterol metabolism through identification of an alpha2beta2 heterotetrameric acyl coenzyme A dehydrogenase family. *J. Bacteriol. 195* (19), 4331−4341.
(28) Yang, M., Lu, R., Guja, K. E., Wipperman, M. F., St Clair, J. R., Bonds, A. C., Garcia-Diaz, M., and Sampson, N. S. (2015) Unraveling cholesterol catabolism in *Mycobacteriumtuberculosis*: ChsE4-ChsE5 alpha2beta2 acyl-CoA dehydrogenase initiates beta-oxidation of 3-oxo-cholest-4-en-26-oyl CoA. *ACS Infect. Dis. 1* (2), 110−125.
(29) van der Geize, R., Grommen, A. W., Hessels, G. I., Jacobs, A. A., and Dijkhuizen, L. (2011) The steroid catabolic pathway of the intracellular pathogen *Rhodococcusequi* is important for pathogenesis and a target for vaccine development. *PLoS Pathog. 7* (8), No. e1002181.
(30) Rengarajan, J., Bloom, B. R., and Rubin, E. J. (2005) Genome-wide requirements for *Mycobacteriumtuberculosis* adaptation and survival in macrophages. *Proc. Natl. Acad. Sci. U. S. A. 102* (23), 8327−8332.
(31) Sassetti, C. M., and Rubin, E. J. (2003) Genetic requirements for mycobacterial survival during infection. *Proc. Natl. Acad. Sci. U. S. A. 100* (22), 12989−12994.
(32) Horinouchi, M., Hayashi, T., Koshino, H., Malon, M., Hirota, H., and Kudo, T. (2014) Identification of 9α-hydroxy-17-oxo-1,2,3,4,10,19-hexanorandrostan-5-oic acid in steroid degradation by *Comamonas testosteroni* TA441 and its conversion to the corresponding 6-en-5-oyl coenzyme a (CoA) involving open reading frame 28 (ORF28)- and ORF30-encoded acyl-CoA dehydrogenases. *J. Bacteriol. 196* (20), 3598−3608.
(33) Otani, H., Lee, Y.-E., Casabon, I., and Eltis, L. D. (2014) -Characterization of p-hydroxycinnamate catabolism in a soil Actinobacterium. *J. Bacteriol. 196* (24), 4293−4303.
(34) Sambrook, J. F., and Russell, D. W. (2000) *Molecular cloning: A laboratory manual*, 3rd ed., Cold Spring Harbor Laboratory Press.
(35) Nakashima, N., and Tamura, T. (2004) Isolation and characterization of a rolling-circle-type plasmid from Rhodococcus erythropolis and application of the plasmid to multiple-recombinant-protein expression. *Appl. Environ. Microbiol. 70* (9), 5557−5568.
(36) van Kessel, J. C., Marinelli, L. J., and Hatfull, G. F. (2008) Recombineering mycobacteria and their phages. *Nat. Rev. Microbiol. 6* (11), 851−857.
(37) Wilkins, D. (2019) gggenes: Draw Gene Arrow Maps in 'ggplot2'. R package version 0.4.0, https://CRAN.R-project.org/package=gggenes.

https://dx.doi.org/10.1021/acs.biochem.0c00005
Biochemistry 2020, 59, 1113−1123

(38) Harrison, K. J., Crecy-Lagard, V., and Zallot, R. (2018) Gene Graphics: a genomic neighborhood data visualization web application. *Bioinformatics 34* (8), 1406−1408.
(39) Lemoine, F., Correia, D., Lefort, V., Doppelt-Azeroual, O., Mareuil, F., Cohen-Boulakia, S., and Gascuel, O. (2019) NGPhylogeny.fr: new generation phylogenetic services for non-specialists. *Nucleic Acids Res. 47* (W1), W260−W265.
(40) Edgar, R. C. (2004) MUSCLE: multiple sequence alignment with high accuracy and high throughput. *Nucleic Acids Res. 32* (5), 1792−1797.
(41) Capella-Gutierrez, S., Silla-Martinez, J. M., and Gabaldon, T. (2009) trimAl: a tool for automated alignment trimming in large-scale phylogenetic analyses. *Bioinformatics 25* (15), 1972−1973.
(42) Guindon, S., Dufayard, J.-F., Lefort, V., Anisimova, M., Hordijk, W., and Gascuel, O. (2010) New algorithms and methods to estimate maximum-likelihood phylogenies: assessing the performance of PhyML 3.0. *Syst. Biol. 59* (3), 307−321.
(43) Lehman, T. C., and Thorpe, C. (1990) Alternate electron acceptors for medium-chain acyl-CoA dehydrogenase: use of ferricenium salts. *Biochemistry 29* (47), 10594−10602.
(44) Franke, D., Petoukhov, M. V., Konarev, P. V., Panjkovich, A., Tuukkanen, A., Mertens, H. D. T., Kikhney, A. G., Hajizadeh, N. R., Franklin, J. M., Jeffries, C. M., and Svergun, D. I. (2017) ATSAS 2.8: a comprehensive data analysis suite for small-angle scattering from macromolecular solutions. *J. Appl. Crystallogr. 50* (4), 1212−1225.
(45) Whiteside, M. D., Winsor, G. L., Laird, M. R., and Brinkman, F. S. (2013) OrthologeDB: a bacterial and archaeal orthology resource for improved comparative genomic analysis. *Nucleic Acids Res. 41* (D1), D366−D376.
(46) Crowe, A. M., Workman, S. D., Watanabe, N., Worrall, L. J., Strynadka, N. C. J., and Eltis, L. D. (2018) IpdAB, a virulence factor in *Mycobacterium tuberculosis*, is a cholesterol ring-cleaving hydrolase. *Proc. Natl. Acad. Sci. U. S. A. 115* (15), E3378−E3387.
(47) Dresen, C., Lin, L. Y. C., D'Angelo, I., Tocheva, E. I., Strynadka, N., and Eltis, L. D. (2010) A Flavin-dependent monooxygenase from *Mycobacterium tuberculosis* involved in cholesterol catabolism. *J. Biol. Chem. 285* (29), 22264−22275.
(48) Wipperman, M. F., Sampson, N. S., and Thomas, S. T. (2014) Pathogen roid rage: cholesterol utilization by *Mycobacterium tuberculosis*. *Crit. Rev. Biochem. Mol. Biol. 49* (4), 269−293.
(49) Griffin, J. E., Gawronski, J. D., Dejesus, M. A., Ioerger, T. R., Akerley, B. J., and Sassetti, C. M. (2011) High-resolution phenotypic profiling defines genes essential for mycobacterial growth and cholesterol catabolism. *PLoS Pathog. 7* (9), No. e1002251.

https://dx.doi.org/10.1021/acs.biochem.0c00005
Biochemistry 2020, 59, 1113−1123